Journal of Power Sources 243 (2013) 859–864

Contents lists available at SciVerse ScienceDirect

Journal of Power Sources

journal homepage: www.elsevier.com/locate/jpowsour

Short communication

Carbon nanotube-embedding $LiFePO_4$ as a cathode material for high rate lithium ion batteries

Jong-Pil Jegal, Kwang-Bum Kim*

Department of Materials Science and Engineering, Yonsei University, 134 Shinchon Dong, Seodaemoon-gu, Seoul 120-749, Republic of Korea

HIGHLIGHTS

- CNTs embedded within $LiFePO_4$ allows for high electronic conductivity.
- Cross-linked CNT imparts interconnected pore structure to the electrode.
- It shows excellent rate capability up to 100 C without additional conducting agent.
- Discharge capacity at 60 C was mainly obtained from the plateau retained above 3.0 V.

ARTICLE INFO

Article history:
Received 8 April 2013
Received in revised form
13 June 2013
Accepted 14 June 2013
Available online 25 June 2013

Keywords:
Carbon nanotube-embedding lithium iron phosphate
Interconnected pore structure
Li-ion battery
Nanocomposites

ABSTRACT

Carbon nanotube-embedding $LiFePO_4$ is synthesized via a solution-based two-step method. The embedded carbon nanotubes are found to improve electron and ion transfer, resulting in excellent high rate capability. An electrode of the nanocomposite, prepared without additional conducting agent, delivers a discharge capacity of 165 mAh g^{-1} at 0.1 C, 120 mAh g^{-1} at 30 C, and 78 mAh g^{-1} at 120 C, based on the weight of $LiFePO_4$. Furthermore, the discharge curve at a discharge rate of 60 C retains the potential plateau above 3.0 V.

1. Introduction

Lithium ion batteries (LIBs) have found application in portable electronic devices and in hybrid electric vehicles (HEVs) and electric vehicles (EVs), which require high power density as well as high energy density. Thus, cathode materials with high specific capacity and high rate capability are in demand [1,2]. $LiFePO_4$ shows promise as a cathode material for HEVs and EVs owing to its high specific capacity, excellent structural stability, environmental benignity, and abundance of Fe [3,4]. However, its poor electronic conductivity (10^{-9} S cm^{-1}) and lithium diffusion rate (10^{-14}–10^{-12} cm^2 s^{-1}) significantly limit its performance at high rates [5–9]. Therefore, recent studies on $LiFePO_4$ have focused on improving its rate capability. Coatings of conductive materials [5–10], doping of supervalent ions [11], and composites with metallic Fe_2P [12] have been reported to improve the electronic conductivity. Solid-state reaction [5,8], and hydro/solvothermal methods [7,13,14] have been used to reduce particle size so as to shorten the travel length of the Li ions and electrons.

Efforts have also been made to improve rate performance of the $LiFePO_4$ using nanocomposites, compromising $LiFePO_4$ nanoparticles and nano-carbons such as carbon nanotubes (CNTs) and graphene [14–16]. These nano-carbons improve the high rate capability of $LiFePO_4$, when they are uniformly dispersed in the composite and are in intimate contact with $LiFePO_4$. Muraliganth et al. used a microwave-solvothermal technique to fabricate a $LiFePO_4$–CNT composite with a capacity of 130 mAh g^{-1} at 10 C [14]. In addition, Zhou et al. used a spray-drying technique to fabricate a $LiFePO_4$/graphene composite with a capacity of 70 mAh g^{-1} at 60 C [16]. However, additional conducting agents were added when fabricating electrodes of such $LiFePO_4$/nano-carbon composites. This is because the electronic conductivities of the composites were low. Therefore, $LiFePO_4$/nano-carbon composites in which the nano-carbon is uniformly dispersed and in

* Corresponding author. Tel.: +82 2 2123 2839; fax: +82 2 312 5375.
E-mail address: kbkim@yonsei.ac.kr (K.-B. Kim).

0378-7753/$ – see front matter © 2013 Elsevier B.V. All rights reserved.
http://dx.doi.org/10.1016/j.jpowsour.2013.06.090

close contact with $LiFePO_4$ are highly desirable as these will obviate the need for extra conducting additive.

In this study, we report the synthesis and electrochemical characterization of CNT-embedding $LiFePO_4$, with the CNT network providing a conduction path. The nanocomposite exhibited a discharge capacity close to its theoretical capacity (165 mAh g^{-1}) at 0.1 C. Moreover, it also exhibited excellent high rate capability with a discharge capacity of 120 mAh g^{-1} at 30 C, 107 mAh g^{-1} at 60 C and 78 mAh g^{-1} even at 120 C without extra conducting agent.

2. Experimental

2.1. Synthesis of CNT-embedding $LiFePO_4$

CNT-embedding $LiFePO_4$ was prepared by a two-step solution-based method. In the first step, a $FePO_4 \cdot H_2O$/CNT coaxial nanocomposite, the precursor for CNT-embedding $LiFePO_4$, was synthesized via a precipitation method [17]. The CNT powder (0.4 g) (Hanhwa Nanotech) was immersed in a urea solution (1.5 M, 720 ml) (eAldrich) and sonicated in an ice bath for 30 min. Then, $FeSO_4 \cdot 7H_2O$ (0.75 M, 24 ml) (Aldrich), citric acid (0.25 M, 8 ml) (Junsei), and $NH_4H_2PO_4$ (0.75 M, 24 ml) (Aldrich) were added sequentially with vigorous stirring. The solution was heated at 60 °C for 3 h. The product was washed repeatedly with distilled water and dried at 60 °C for 24 h. The as-synthesized $FePO_4 \cdot 4H_2O$/CNT was heat treated at 300 °C for 6 h to obtain $FePO_4 \cdot H_2O$/CNT, with the hydrated water decreasing from 4 to 1. In the second step, $FePO_4 \cdot H_2O$/CNT was chemically lithiated in a 2 M LiI solution in acetonitrile for 24 h in an Ar-filled glove box. The product was washed with acetone and dried at 60 °C for 12 h. It should be noted that the acetone was used as washing solvent instead of acetonitrile because it is more inexpensive and easier to handle than acetonitrile, and there was little change in the physicochemical properties of the synthesized material. The dried powder was heat-treated at 700 °C for 3 h in an Ar/H_2 (95:5) atmosphere to obtain CNT-embedding $LiFePO_4$.

2.2. Characterization

The morphologies of $FePO_4 \cdot H_2O$/CNT and CNT-embedding $LiFePO_4$ were examined using field emission scanning electron microscopy (FE-SEM; Hitachi, S-4300). Their structures were characterized via X-ray diffraction (XRD; Rigaku D/MAX 2200V/PC) analysis, with the diffraction data being collected over 2θ of 10–80°. Thermo-gravimetric analysis and differential thermal analysis (TGA–DTA; Bruker 2010SA) were used to determine the loading amount of $LiFePO_4$ in CNT-embedding $LiFePO_4$. The analysis was performed in air over temperature ranging room temperature to 700 °C, with the heating rate of 10 °C min^{-1}.

2.3. Electrochemical measurements

Cyclic voltammetry was performed using a three-electrode electrochemical cell; two lithium metal foils were used as the counter and reference electrodes. Galvanostatic charge/discharge tests were performed using a coin cell (2032), with lithium foil as the counter electrode. The working electrode was prepared by mixing 95 wt.% of CNT-embedding $LiFePO_4$ and 5 wt.% of polyvinylidene fluoride (PVDF; Aldrich), used as a binder, dissolved in *N*-methyl-pyrrolidone (NMP; Aldrich), with no additional conducting agent being used. The slurry was coated on an aluminum foil, dried, and then, roll-pressed. The amount of slurry used to form the electrode was about 2 mg cm^{-2}. A potentiostat/galvanostat (MPG2, Bio-logic) was used for the cyclic voltammetry and charge/discharge tests. The cut-off voltages were 2.0–4.3 V versus Li/Li^+. Electrochemical impedance spectroscopy (EIS) measurements were carried out using potentiostat/galvanostat (VMP2, Bio-logic) over the frequency range from 100 kHz to 10 mHz with AC signal of 5 mV. The electrolyte was a 1 M $LiPF_6$ dissolved in a mixture of ethyl carbonate (EC) and dimethyl carbonate (DMC) in a volume ratio of 1:1.

3. Results and discussion

Fig. 1a shows an SEM image of $FePO_4 \cdot H_2O$/CNT coaxial nanocomposite, the precursor for the synthesis of CNT-embedding $LiFePO_4$. As can be seen, the entire surface of CNT is covered with $FePO_4 \cdot H_2O$, leading to the formation of a coaxial-type nanocomposite. The TEM image in Fig. 1b shows the coaxial nature of the precursor, with the CNTs being encased within a ~25-nm-thick $FePO_4 \cdot H_2O$ layer. This proves that $FePO_4 \cdot H_2O$ precipitated only on the CNT surfaces, through heterogeneous nucleation and growth during the synthesis process, with there being no trace of homogeneously nucleated $FePO_4 \cdot H_2O$ nanoparticles in the solution [17].

Fig. 2a shows an SEM image of CNT-embedding $LiFePO_4$, in which the precipitate morphology in $FePO_4 \cdot H_2O$/CNT changed, transforming from thin $FePO_4 \cdot H_2O$ layers on the CNTs' surfaces to irregular-shaped $LiFePO_4$ nanoparticles 100–200 nm in size upon lithiation. This transformation, which is occurred in the chemical lithiation, not in the heat treatment, suggested that a dissolution and re-precipitation mechanism caused the formation of the $LiFePO_4$ nanoparticles through the chemical lithiation of $FePO_4$. Since the $LiFePO_4$ particles in CNT-embedding $LiFePO_4$ were larger in size than the thickness of the $FePO_4$ layer in $FePO_4 \cdot H_2O$/CNT, it can be assumed that some of the CNTs were not buried in the

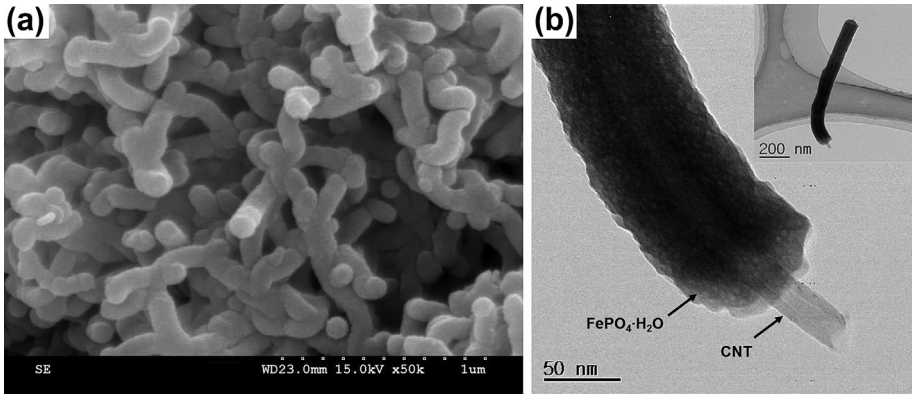

Fig. 1. (a) SEM image and (b) TEM image of $FePO_4 \cdot H_2O$/CNT, the precursor for the synthesis of CNT-embedding $LiFePO_4$.

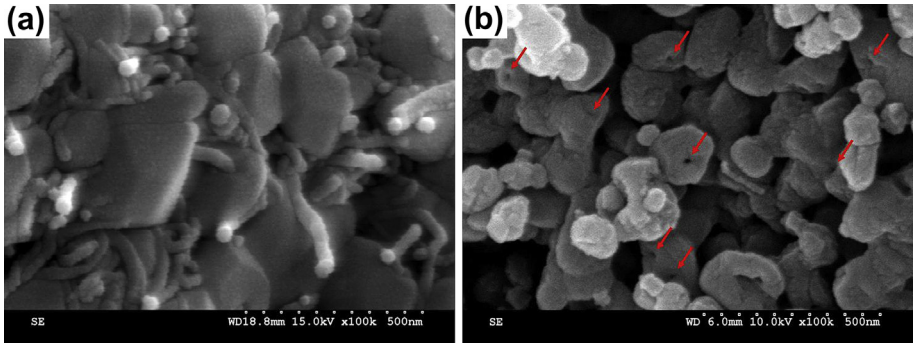

Fig. 2. (a) SEM image of the CNT-embedding $LiFePO_4$ and (b) SEM image of the $LiFePO_4$ nanoparticles after the embedded CNTs had been burnt away in air.

$LiFePO_4$ particles and were exposed. The cross-linked CNTs in CNT-embedding $LiFePO_4$ imparts an interconnected pore structure, which acts as a continuous pathway for the electrolyte ions, resulting in enhanced access of Li ions throughout the structure [18]. In order to confirm the formation of such a structure, CNT-embedding $LiFePO_4$ was heat treated at 500 °C for 6 h in air to burn away the CNTs present. It can be seen from Fig. 2b that some of the heat treated $LiFePO_4$ particles are bead-like and have holes through their middles (as marked), which is evidence of the CNT-embedding structure of the synthesized nanocomposite. In addition, the fact that these pores were formed in and around the $LiFePO_4$ particles in the areas initially occupied by CNTs is proof of the existence of a network of cross-linked CNTs in the nanocomposite. CNT-embedded structure can also be identified with TEM images shown in supplementary data. Fig. S1 shows that the $LiFePO_4$ nanoparticles have holes through their middles, that is, the trace of the embedded CNTs, which is the same as the SEM observation in Fig. 2b. In addition, it can be seen that the hollow-shaped $LiFePO_4$ nanoparticles is found in TEM images in Fig. S2. From this result, it can be concluded that the exposed CNTs in Fig. 2a are partially coated with nanometer-thick $LiFePO_4$ nanoparticles, which can be favorable for the high rate capability due to the short diffusion distance of Li^+ ions and good electrical conductivity.

Fig. 3a shows XRD patterns of $FePO_4 \cdot H_2O$/CNT, which indicates that the $FePO_4 \cdot H_2O$ in the precursor was amorphous. These patterns exhibit broadened and merged peaks, in the same positions as the characteristic peaks of $FePO_4$ (JCPDS card No. 29-0715). It should be noted that the amorphous nature of $FePO_4 \cdot H_2O$ is critical to the preparation of $LiFePO_4$, since amorphous $FePO_4 \cdot H_2O$ exhibits a higher activity with respect to chemical lithiation than do its crystalline phases, such as trigonal and hexagonal [19]. In contrast, the XRD pattern of CNT-embedding $LiFePO_4$ in Fig. 3b exhibits a series of sharp diffraction peaks that indicate high crystallinity; corresponds to that of single-phased olivine (JCPDS card No. 40-1499). The broad hump noticed in both XRD spectra over 25–27° can be attributed to the CNTs.

Fig. 4a shows the TGA–DTA curves of the $FePO_4 \cdot H_2O$/CNT precursor. A broad endothermic peak in a range of 80–300 °C, corresponding to the removal of structural water, continued up to the temperatures of around 500 °C with a weight loss of 8.2%. As the temperature was raised to 620 °C, another strong exothermic peak appeared. It was attributed to the burn-out of CNT, since bare CNTs burnt away and exhibited an exothermic peak at 650 °C, as shown in Fig. 4b. The resulting amount of $FePO_4 \cdot H_2O$ in the precursor was 76.7 wt.%. The TGA–DTA curves of the CNT-embedding $LiFePO_4$ are shown in Fig. 4c. It exhibits a small exothermic peak at 360 °C owing to oxidation of $LiFePO_4$ to $Li_3Fe_2(PO_4)_3$ and Fe_2O_3 [7], with a weight gain of 2.6%. Additionally, two strong exothermic peaks are observed at around 530 and 635 °C, and attributed to the burn-out of CNT. As in the case of TGA–DTA curves of the $FePO_4 \cdot H_2O$/CNT and the bare CNTs, the peak at 635 °C was clearly due to the burn-out of CNTs in the composite. It has been reported that oxidation of the $LiFePO_4$ is initiated at about 300 °C and completed at 550 °C [7]. The oxidation reaction is accompanied by a release of exothermic heat, causing a local temperature increase in the sample. Therefore, it is highly probable that the embedded CNTs in direct contact with $LiFePO_4$

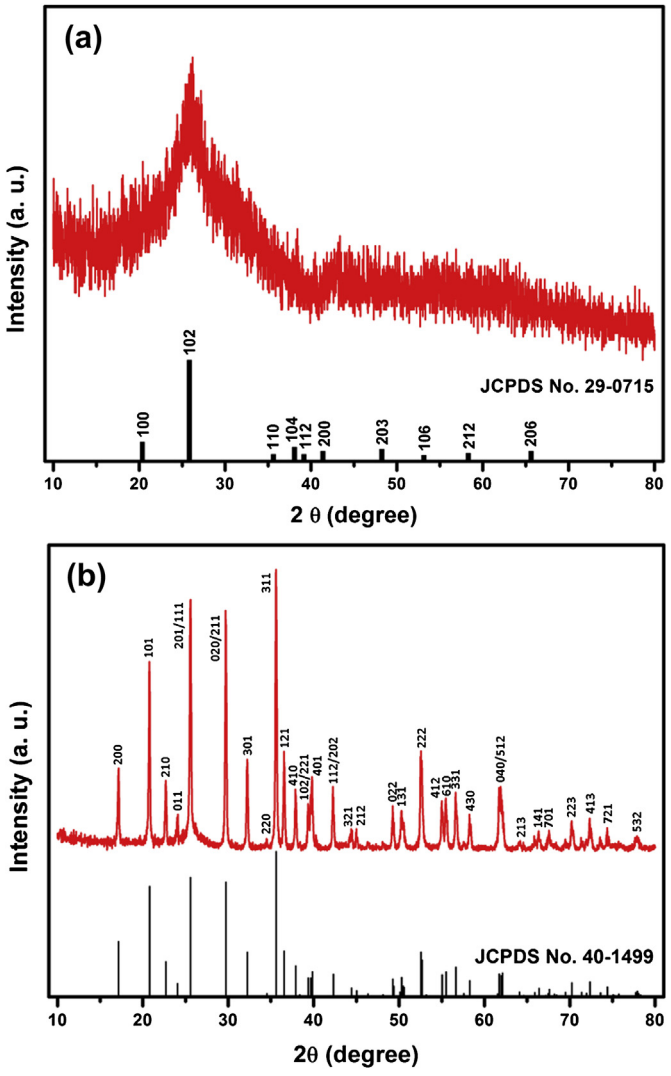

Fig. 3. XRD patterns of (a) $FePO_4 \cdot H_2O$/CNT and (b) CNT embedding $LiFePO_4$.

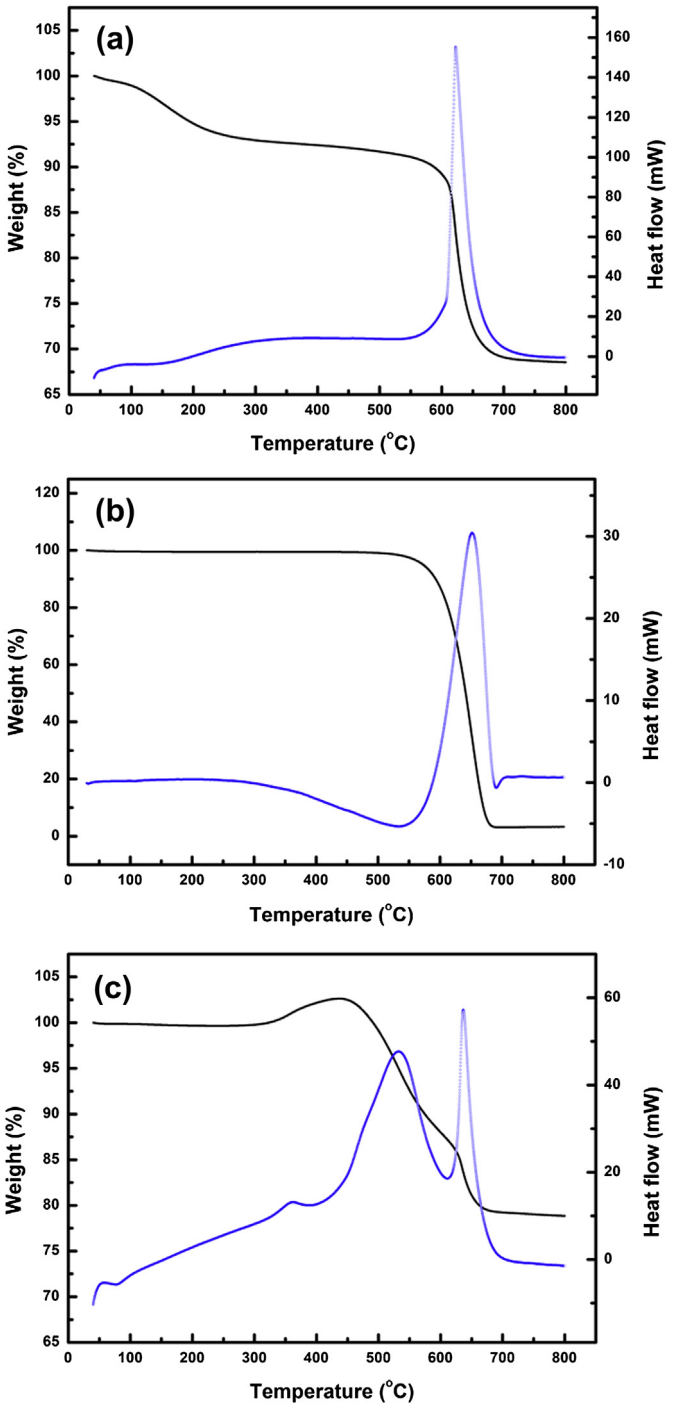

Fig. 4. TGA–DTA curves of (a) $FePO_4 \cdot H_2O$/CNT, (b) bare CNTs, and (c) CNT embedding $LiFePO_4$.

might be burnt out at lower temperatures than those of $FePO_4 \cdot H_2O$/CNT and the bare CNTs. Finally, the amount of the resulting powder composed of $Li_3Fe_2(PO_4)_3$ and Fe_2O_3 was 78.8 wt.% after TGA–DTA measurement. As a result, the amount of $LiFePO_4$ in the CNT-embedding $LiFePO_4$ was calculated to be 76.2 wt.% (78.8 wt.%–2.6 wt.%). Given that the $FePO_4 \cdot H_2O$ content in $FePO_4 \cdot H_2O$/CNT was 76.7 wt.%, the amount of $LiFePO_4$ in CNT-embedding $LiFePO_4$ was 76.2 wt.%, which is in good agreement with the theoretical calculation (76.4 wt.%) based on the hydration water removal from $FePO_4 \cdot H_2O$, while also considering the formation of $LiFePO_4$ via lithiation.

Fig. 5a shows cyclic voltammograms (CVs) of CNT-embedding $LiFePO_4$, measured at potential scan rates of 0.5–15 mV s^{-1}. The CV at 0.5 mV s^{-1} (inset) shows a set of well-defined peaks: an oxidation peak at 3.57 V ($LiFePO_4 \rightarrow FePO_4 + Li^+ + e^-$) and a reduction peak at 3.27 V ($FePO_4 + Li^+ + e^- \rightarrow LiFePO_4$). The shapes of the peaks in the CVs remained unchanged even at potential scan rates as high as 15 mV s^{-1}. This is indicative of the excellent high rate capability of CNT-embedding $LiFePO_4$. To our knowledge, no previous study has reported the CV for $LiFePO_4$ at such a high potential scan rate when used as a slurry electrode, except during investigations made using a cavity microelectrode (CME) [20]. However, since only a few micrograms of the $LiFePO_4$ mixture, which contained 50 wt.% of a conducting agent, was used to form the CME, we chose not to compare the rate capabilities obtained using CME with those obtained in this study.

The apparent diffusion coefficient (D_{app}) of Li^+ ions in the CNT-embedding $LiFePO_4$ was calculated using the Randles–Sevcik equation:

$$I_p/m = 0.4463F(F/RT)^{0.5}A_e(D_{app})^{0.5}C_{Li}^{*}\nu^{0.5} \quad (1)$$

where I_p is the peak current in amperes, m is the mass of the electrode, F is the Faraday constant, A_e is the surface area of the electrode area per unit mass ($cm^2\ g^{-1}$), C_{Li}^{*} is the initial concentration of Li in $LiFePO_4$ (0.0228 mol cm^{-3}), ν is scan rate in V s^{-1}, and D_{app} is the apparent diffusion coefficient [21]. It should be noted that surface area used in the calculation was for the residual particles after the embedded CNTs had been burnt out in air (8.9 $m^2\ g^{-1}$) since the surface area of the CNT-embedding $LiFePO_4$ was abnormally large because of the presence of the CNTs (85.9 $m^2\ g^{-1}$). In addition, one-third of the surface area was used as effective surface area because of one-dimensional diffusion path of Li^+ ions in the $LiFePO_4$ [21]. The calculated anodic and cathodic apparent diffusion coefficients were 4.39×10^{-13} and 3.23×10^{-13} $cm^2\ s^{-1}$, respectively. The obtained values are within the reported results [22].

Fig. 5b shows galvanostatic charge/discharge curves of CNT-embedding $LiFePO_4$ at C-rates of 0.1–120 C. It should be noted that the charge/discharge tests were performed at the same C-rates. The CNT-embedding $LiFePO_4$ electrode, which was prepared without adding a conducting agent, exhibited flat charge/discharge potential plateaus and a specific discharge capacity of 165 mAh g^{-1} at a discharge rate of 0.1 C. This was determined on the basis of the weight of $LiFePO_4$ in the electrode, which corresponded to 97% of the theoretical capacity of $LiFePO_4$. This was attributed to the highly crystalline and single-phase of $LiFePO_4$ and to the availability of a conduction path owing to the intimate contact between the $LiFePO_4$ nanoparticles and the CNTs, all of which allowed for a high degree of electrochemical utilization of $LiFePO_4$. This led to the high specific discharge capacity of $LiFePO_4$ being close to its theoretical capacity. At higher charge/discharge rates, CNT-embedding $LiFePO_4$ exhibited excellent high rate capability. It could deliver a discharge capacity of 139 mAh g^{-1} (84% of the initial capacity at 0.1 C) at a discharge rate of 10 C and 107 mAh g^{-1} (65%) at 60 C. Moreover, it could deliver a discharge capacity of 78 mAh g^{-1} (47%) at a rate as high as 120 C, which corresponded to a charge/discharge time of 30 s. In addition, it is worth noting that a significant part of the discharge capacity at 60 C was obtained from the potential plateau retained above 3.0 V. Therefore, CNT-embedding $LiFePO_4$ can sustain not only a high discharge capacity, but also a high discharge voltage, at high rate operations. Recently, several papers have reported on $LiFePO_4$, claiming enhanced rate capabilities. However, most of the discharge capacities observed at high C rates arose from

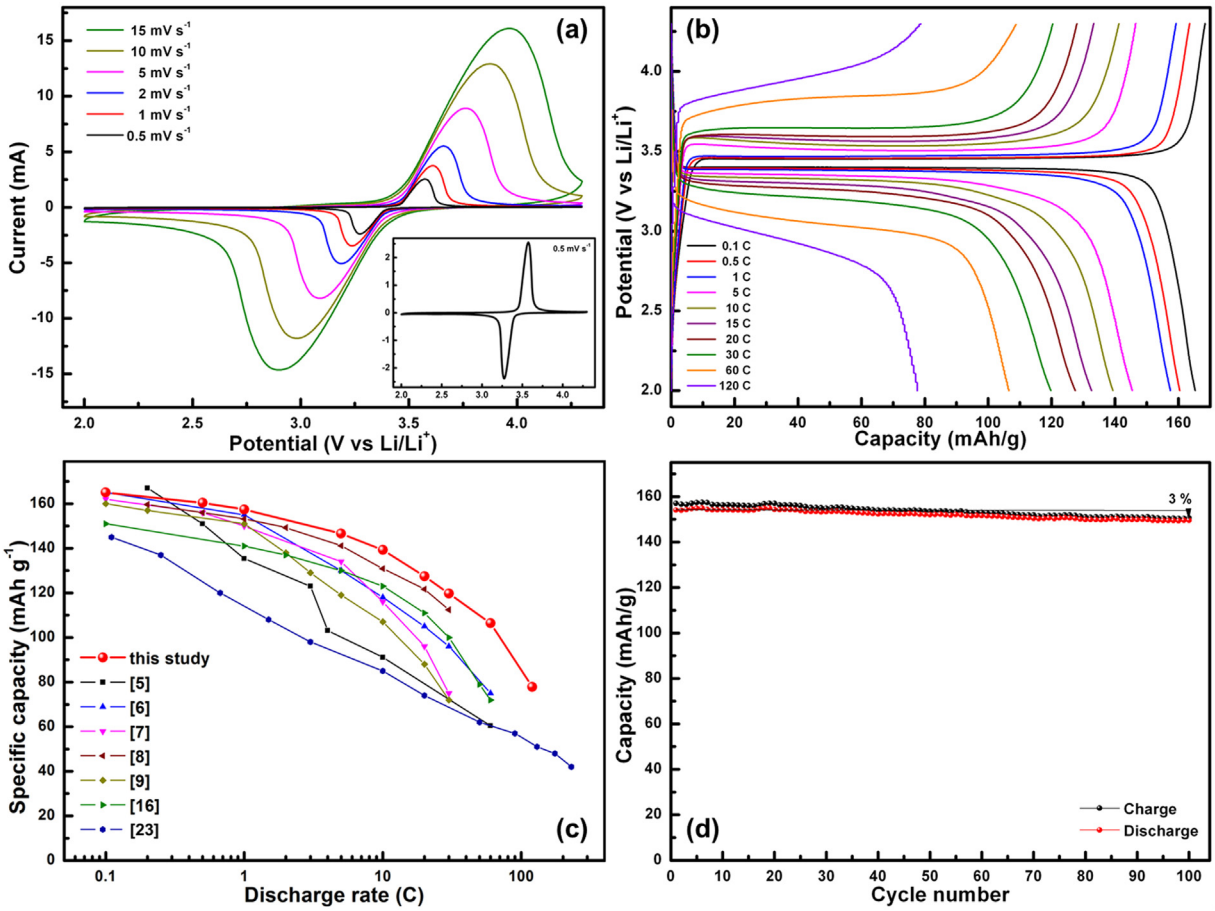

Fig. 5. (a) Cyclic voltammograms of the CNT-embedding $LiFePO_4$ electrode at scan rates of 0.5–15 mV s^{-1}, (b) charge–discharge profiles of the electrode at high C rates for cut-off voltages of 2.0–4.3 V, (c) high rate capability of the electrode and those reported previously, and (d) specific capacity of the electrode with the number of cycles at 1 C-rate.

sloping discharge region below 3.0 V [7–9,16,23]. Therefore, the CNT-embedding $LiFePO_4$ is superior to those with sloping discharge curves in terms of power density and energy density at high discharge C rates.

Fig. 5c compares the high rate capability of the CNT-embedding $LiFePO_4$ with those reported previously [5–9,16,23]. Of these, the electrodes prepared with carbon coated $LiFePO_4$ nanoparticles [6,7] and graphene modified $LiFePO_4$ [16], which used a conductive carbon content in the similar amount as that used in this study, exhibited fairly good rate performances. The CNT-embedding $LiFePO_4$, however, exhibited a markedly better high rate capability over the range of discharge rate up to 100 C. This excellent rate performance may be attributed to the high electronic conductivity of CNT-embedding $LiFePO_4$, which was owing to the embedded CNTs, and to the facile transport of ions through the interconnected pore structure of cross-linked CNTs. This can be supported by the result of EIS measurement as shown in Fig. S3. The CNT-embedding $LiFePO_4$ exhibited quite smaller charge transfer resistance compared to the $LiFePO_4$–CNT mixture although adding amount of CNTs in the mixture was the same as that in the CNT-embedding $LiFePO_4$. This result indicates that the excellent rate performance of the CNT-embedding $LiFePO_4$ is not because of the large amount of the CNTs, but because of uniformly incorporated and embedded structure of the CNTs. Furthermore, the capacity of CNT-embedding $LiFePO_4$ faded by only 3% after 100 cycles at a charge/discharge rate of 1 C (Fig. 5d), indicating excellent structural stability of the CNT-embedding $LiFePO_4$ during repeated cycling.

4. Conclusion

CNT-embedding $LiFePO_4$ is synthesized via a solution-based two-step method. The CNTs embedded within $LiFePO_4$ nanoparticles allows for the facile transfer of electrons and ions because of their high electronic conductivity and the interconnected pore structure of cross-linked CNTs, respectively. Owing to these electronic and structural properties, the CNT-embedding $LiFePO_4$ has an excellent high rate capability. An electrode of the nanocomposite, prepared without extra conducting agent, can deliver a discharge capacity of 165 mAh g^{-1} at 0.1 C, 120 mAh g^{-1} at 30 C, and 78 mAh g^{-1} at 120 C, based on the weight of $LiFePO_4$. Furthermore, the discharge curve at a discharge rate of 60 C retains the potential plateau above 3.0 V.

Acknowledgements

This work was supported by the energy efficiency and resources of the Korea Institute of Energy Technology Evaluation and Planning (KETEP) grant funded by the Ministry of Knowledge Economy, Korean government (No: 20122010100140), and also supported by POSCO.

Appendix A. Supplementary data

Supplementary data related to this article can be found at http://dx.doi.org/10.1016/j.jpowsour.2013.06.090.

References

[1] J.W. Fergus, J. Power Sources 195 (2010) 939–954.
[2] P. Gibot, M. Casas-Cabanas, L. Laffont, S. Levasseur, P. Carlach, S. Hamelet, J.-M. Tarascon, C. Masquelier, Nat. Mater. 7 (2008) 741–747.
[3] A.K. Padhi, K.S. Nanjundaswamy, J.B. Goodenough, J. Electrochem. Soc. 144 (1997) 1188–1194.
[4] S.F. Yang, P.Y. Zavalij, M.S. Whittingham, Electrochem. Commun. 3 (2001) 505–508.
[5] X.L. Yang, F. Mou, L.L. Zhang, G. Peng, Z.X. Dai, Z.Y. Wen, J. Power Sources 204 (2012) 182–186.
[6] M. Konarova, I. Taniguchi, J. Power Sources 195 (2010) 3661–3667.
[7] X.M. Lou, Y.X. Zhang, J. Mater. Chem. 21 (2011) 4156–4160.
[8] F.Q. Cheng, W. Wan, Z. Tan, Y.Y. Huang, H.H. Zhou, J.T. Chen, X.X. Zhang, Electrochim. Acta 56 (2011) 2999–3005.
[9] Y.H. Huang, H.B. Ren, S.G. Yin, Y.H. Wang, Z.H. Peng, Y.H. Zhou, J. Power Sources 195 (2010) 610–613.
[10] Y.H. Huang, J.B. Goodenough, Chem. Mater. 20 (2008) 7237–7241.
[11] N. Meethong, Y.H. Kao, S.A. Speakman, Y.M. Chiang, Adv. Funct. Mater. 19 (2009) 1060–1070.
[12] C.W. Kim, J.S. Park, K.S. Lee, J. Power Sources 163 (2006) 144–150.
[13] A.V. Murugan, T. Muraliganth, A. Manthiram, J. Phys. Chem. C 112 (2008) 14665–14671.
[14] T. Muraliganth, A.V. Murugan, A. Manthiram, J. Mater. Chem. 18 (2008) 5661–5668.
[15] Y.K. Zhou, J. Wang, Y.Y. Hu, R. O'Hayre, Z.P. Shao, Chem. Commun. 46 (2010) 7151–7153.
[16] X.F. Zhou, F. Wang, Y.M. Zhu, Z.P. Liu, J. Mater. Chem. 21 (2011) 3353–3358.
[17] J.P. Jegal, J.G. Kim, K.B. Kim, Electrochem. Commun. 30 (2013) 87–90.
[18] A.E. Fischer, K.A. Pettigrew, D.R. Rolison, R.M. Stroud, J.W. Long, Nano Lett. 7 (2007) 281–286.
[19] Y. Song, S.F. Yang, P.Y. Zavalij, M. Stanley Whittingham, Mater. Res. Bull. 37 (2002) 1249–1257.
[20] J. Come, P.-L. Taberna, S. Hamelet, C. Masquelier, P. Simon, J. Electrochem. Soc. 158 (2011) A1090–A1093.
[21] Y.W. Yu, C. Fietzek, W. Weydanz, K. Donoue, T. Inoue, H. Kurokawa, S. Fujitani, J. Electrochem. Soc. 154 (2007) A253–A257.
[22] M.G. Park, X.C. Zhang, M.D. Chung, G.B. Less, A.M. Sastry, J. Power Sources 195 (2010) 7904–7929.
[23] X.L. Wu, L.Y. Jiang, F.F. Cao, Y.G. Guo, L.J. Wan, Adv. Mater. 21 (2009) 2710–2714.